AFRL-RY-WP-TR-2018-0114

POLARITONIC HOT-ELECTRON INFRARED PHOTODETECTOR (PHIP) AT THE WAFER SCALE

Jon-Paul Maria
North Carolina State University

Sanjay Krishna
Ohio State University

Christopher Shelton
Third Floor Materials, Inc.

SEPTEMBER 2018
Final Report

Approved for public release; distribution is unlimited.

See additional restrictions described on inside pages

STINFO COPY

AIR FORCE RESEARCH LABORATORY
SENSORS DIRECTORATE
WRIGHT-PATTERSON AIR FORCE BASE, OH 45433-7320
AIR FORCE MATERIEL COMMAND
UNITED STATES AIR FORCE

NOTICE AND SIGNATURE PAGE

Using Government drawings, specifications, or other data included in this document for any purpose other than Government procurement does not in any way obligate the U.S. Government. The fact that the Government formulated or supplied the drawings, specifications, or other data does not license the holder or any other person or corporation; or convey any rights or permission to manufacture, use, or sell any patented invention that may relate to them.

This report is the result of contracted fundamental research deemed exempt from public affairs security and policy review in accordance with SAF/AQR memorandum dated 10 Dec 08 and AFRL/CA policy clarification memorandum dated 16 Jan 09. This report is available to the general public, including foreign nationals.

Copies may be obtained from the Defense Technical Information Center (DTIC) (http://www.dtic.mil).

AFRL-RY-WP-TR-2018-0114 HAS BEEN REVIEWED AND IS APPROVED FOR PUBLICATION IN ACCORDANCE WITH ASSIGNED DISTRIBUTION STATEMENT.

// Signature//

GAMINI ARIYAWANSA, Program Manager
Optoelectronics Technology Branch
Aerospace Components & Subsystems Division

// Signature//

FRED E. ARNOLD, Chief
Optoelectronics Technology Branch
Aerospace Components & Subsystems Division

// Signature//

RANDALL D. DEPPENSMITH, Lt Col, USAF
Deputy
Aerospace Components & Subsystems Division
Sensors Directorate

This report is published in the interest of scientific and technical information exchange, and its publication does not constitute the Government's approval or disapproval of its ideas or findings.

*Disseminated copies will show "//Signature//" stamped or typed above the signature blocks.

REPORT DOCUMENTATION PAGE

Form Approved
OMB No. 0704-0188

The public reporting burden for this collection of information is estimated to average 1 hour per response, including the time for reviewing instructions, searching existing data sources, gathering and maintaining the data needed, and completing and reviewing the collection of information. Send comments regarding this burden estimate or any other aspect of this collection of information, including suggestions for reducing this burden, to Department of Defense, Washington Headquarters Services, Directorate for Information Operations and Reports (0704-0188), 1215 Jefferson Davis Highway, Suite 1204, Arlington, VA 22202-4302. Respondents should be aware that notwithstanding any other provision of law, no person shall be subject to any penalty for failing to comply with a collection of information if it does not display a currently valid OMB control number. **PLEASE DO NOT RETURN YOUR FORM TO THE ABOVE ADDRESS**.

1. REPORT DATE ***(DD-MM-YY)***
September 2018

2. REPORT TYPE
Final

3. DATES COVERED ***(From - To)***
16 May 2017 – 16 May 2018

4. TITLE AND SUBTITLE
POLARITONIC HOT-ELECTRON INFRARED PHOTODETECTOR (PHIP) AT THE WAFER SCALE

5a. CONTRACT NUMBER
FA8650-17-1-7700

5b. GRANT NUMBER

5c. PROGRAM ELEMENT NUMBER
62716E

6. AUTHOR(S)
Jon-Paul Maria (North Carolina State University)
Christopher Shelton (Third Floor Materials, Inc. (3FM))
Sanjay Krishna (Ohio State University (OSU))

5d. PROJECT NUMBER
N/A

5e. TASK NUMBER
N/A

5f. WORK UNIT NUMBER
Y1L5

7. PERFORMING ORGANIZATION NAME(S) AND ADDRESS(ES)

North Carolina State University
1001 Capability Drive
Raleigh, NC 27695

3FM
310 South Harrington
Raleigh, NC 27603

OSU
205 Dreese Laboratories
2015 Neil Aveue
Columbus, OH 43201

8. PERFORMING ORGANIZATION REPORT NUMBER

9. SPONSORING/MONITORING AGENCY NAME(S) AND ADDRESS(ES)

Air Force Research Laboratory
Sensors Directorate
Wright-Patterson Air Force Base, OH 45433-7320
Air Force Materiel Command
United States Air Force

Defense Advanced
Research Projects Agency
DARPA/MTO
675 North Randolph Street
Arlington, VA 22203

10. SPONSORING/MONITORING AGENCY ACRONYM(S)
AFRL/RYDH

11. SPONSORING/MONITORING AGENCY REPORT NUMBER(S)
AFRL-RY-WP-TR-2018-0114

12. DISTRIBUTION/AVAILABILITY STATEMENT
Approved for public release; distribution is unlimited.

13. SUPPLEMENTARY NOTES
This report is the result of contracted fundamental research deemed exempt from public affairs security and policy review in accordance with SAF/AQR memorandum dated 10 Dec 08 and AFRL/CA policy clarification memorandum dated 16 Jan 09. This material is based on research sponsored by Air Force Research laboratory (AFRL) and the Defense Advanced Research Agency (DARPA) under agreement number FA8650-17-1-7700. The U.S. Government is authorized to reproduce and distribute reprints for Governmental purposes notwithstanding any copyright notation herein. The views and conclusions contained herein are those of the authors and should not be interpreted as necessarily representing the official policies of endorsements, either expressed or implied, of AFRL and the DARPA or the U.S. Government. Report contains color.

14. ABSTRACT
Third Floor Materials, Inc. (3FM) addressed the need for low-cost, high throughput sensor fabrication with a revolutionary new material technology that plasmonically couples infrared light into an electrical signal. Over the course of a one-year program, 3FM demonstrated the fundamental science behind and explored the performance envelope of a new sensor utilizing plasmonic coupling in donor-doped cadmium oxide (CdO). The Photoemissive Heterostructure Infrared Photodetector (PHIP) concept overcomes challenges associated with traditional Schottky barrier detectors and shows promise as a potential high-operating temperature sensor.

15. SUBJECT TERMS
photodectector, infrared, polaritonic, internal photoemission, cadmium oxide

16. SECURITY CLASSIFICATION OF:			17. LIMITATION OF ABSTRACT:	18. NUMBER OF PAGES	19a. NAME OF RESPONSIBLE PERSON (Monitor)
a. REPORT	b. ABSTRACT	c. THIS PAGE			
Unclassified	Unclassified	Unclassified	SAR	37	Gamini Ariyawansa **19b. TELEPHONE NUMBER** *(Include Area Code)* N/A

Table of Contents

Section **Page**

List of Figures ii
1. EXECUTIVE SUMMARY 1
2. BACKGROUND 3
   2.1 IR Plasmonics 3
   2.2 R:CdO – an Enabling Plasmonic Infrared Material 4
   2.3 CdO Light Matter Interaction – ENZ Modes 5
   2.4 Internal Photoemission 7
3. PHASE I TECHNICAL OBJECTIVES 10
4. PHASE I PROGRAM RESULTS 11
   4.1 Analysis of SBH, Long-Wave Cutoff, and Diode Performance 11
   4.2 Understanding Dark Current in PHIP Devices 13
   4.3 Tuning of Optical Resonance across the MWIR 14
   4.4 Improving Device Performance 16
   4.5 Development of a Custom ROIC 21
   4.6 Successful Experimental Demonstration of the PHIP Device Concept 24
5. OUTLOOK FOR THE PHIP DEVICE 29
6. REFERENCES 30
LIST OF ABBREVIATIONS, ACRONYMS, AND SYMBOLS 31

Approved for public release; distribution is unlimited.

List of Figures

Figure **Page**

Figure 1: Schematic Illustration of Photoemission by Hot Carrier Injection from Plasmonic Decay 4
Figure 2: Carrier Density and Mobility for Sputtered CdO Thin Films Donor-doped with various Cations 5
Figure 3: Illustration showing the Relationship between IR Wavelength and the Thickness of ENZ Layer in which perfect Absorption occurs 6
Figure 5: Schematic of the Band Lineup Measured by XPS for a CdO Film on Silicon 11
Figure 6: Temperature Dependent I-V Properties of CdO-Si Heterojunctions for (a) As-received Silicon; (b) Oxide Strip and Clean; and (c) Ion-beam Modified 12
Figure 7: Richardson Plots for a representative CdO|Si SBD in Forward (a) and Reverse (b) Bias 12
Figure 8: Temperature Dependent Current Density vs. Voltage for a Representative CdO|Si Heterojunction 14
Figure 9: (a) Dual Magnetron Reactive Sputtering System for CdO Deposition and (b) Carrier Concentration and Mobility for Sputtered Films on Silicon 15
Figure 10: Reflectance measured by IR Ellipsometry for a Series of Films will vary Carrier Concentration on Silicon 16
Figure 11: Typical 3FM Measurement Setup for PHIP Tests 17
Figure 12: PHIP Device Photoresponse Improvement over Program Period-of-Performance ... 17
Figure 13: (a) TCAD I-V Response for CdO//Si SBD with Series Resistances of 1μΩ, 100 Ω, 1.2 kΩ, and 10 kΩ; (b) Schematic of Improved, Room-temperature Ca-Al-Au Metal Stack for Ohmic Silicon Contact; and (c) Measured I-V Characteristics for In-Al and Ca-Al back Contacts 18
Figure 14: (a) Schematic of PHIP Single-Element Detector with Extraction Grid on Wafer Backside and (b) Checkplot of various Grid Geometries explored for Extraction Grid Optimization 19
Figure 15: Schematic Illustration of the effect of Backside Roughness in Scattering Light Back towards the Interface 20
Figure 16: Equivalent Circuit for a Generic Photoconductor 21
Figure 17: Simple Test Circuit for PHIP Devices 22
Figure 18: Schematic of the Amplifier fabricated for PHIP Measurements under Bias 23
Figure 19: Calculating Transfer Function of the PHIP Read Out Circuit depicted in Figure 18 23
Figure 20: Schematic of the Measurement Setup used to Measure the PHIP Spectral Responsivity 26
Figure 21: Measured Spectral Responsivity of a Test Device in the Infrared (top) and Measured Responsivity matches the Absorption Spectrum of the Device (bottom) 27
Figure 22: Bias Dependent Response of a PHIP Device 28
Figure 23: Advantage of the PHIP Device in two Panels 29

Approved for public release; distribution is unlimited.

1. EXECUTIVE SUMMARY

Infrared systems and technologies form a backbone of our nations national defense strategy, allowing U.S. warfighters to "Own the Environment" across any terrain, in any weather or lighting condition. It is imperative that the U.S. maintain a technological lead over its near-peer adversaries by continually improving infrared search and track (IRST) systems and sensors. Despite huge investment and the obvious need, however, current infrared (IR) systems rely on materials that were state-of-the-art 50 years ago. Maintaining a technology advantage requires that the Department of Defense (DoD) think outside the realm of traditional materials and investigate new and disruptive possibilities for IR sensors that address not only the capability of a system, *but also its cost.*

Third Floor Materials, Inc. (3FM) seeks to address the need for low-cost, high throughput sensor fabrication with a revolutionary new material technology that plasmonically couples infrared light into an electrical signal. The device design itself relies on established DoD IR technology and fabrication routes, namely internal photoemission (IPE) Si-based Schottky barrier devices, but uses an enabling new material (donor-doped cadmium oxide (CdO)) to facilitate the light absorption and conversion process. Unique material properties result in an effective 'photonic compression' that allows for perfect absorption of IR light in sub-micron thin-films. Coupled with a favorable band structure for emission and high E-field confinement within the absorber, we estimate these new CdO based Schottky barrier detectors will have a 10x quantum efficiency advantage over existing PtSi designs. Most programmatically relevant, however, CdO can be deposited and processed *directly on silicon at complementary metal-oxide-semiconductor (CMOS) compatible temperatures*. In the context of the Defense Advanced Research Projects Agency (DARPA) Wafer Scale Infrared Detectors (WIRED) program, this is an enabling feature, allowing direct integration of the sensor material with the readout integrated circuit (ROIC) and eliminating costly hybridization steps.

Over the course of a one-year DARPA/Air Force Research Laboratory (AFRL) program, 3FM demonstrated the fundamental science behind and explored the performance envelope of a new sensor utilizing plasmonic coupling in donor-doped CdO. The **P**hotoemissive **H**eterostructure **I**nfrared **P**hotodetector (PHIP) concept overcomes challenges associated with traditional Schottky barrier detectors and shows promise as a potential high-operating temperature sensor. We highlight some of the key successes of the program:

1) Development of a physical vapor deposition (PVD) doped-CdO deposition process compatible with silicon
2) Validation of continuously tunable, narrow-band IR absorption in CdO/Si heterostructures
3) Demonstration of CdO/Si Schottky barrier IR detectors
4) Evidence of signal-to-noise greater than 1 in room-temperature operation
5) The first observation of an IR spectral response mediated by an epsilon-near-zero mode

PHIP sensors may have important applications throughout the DoD and we submit further development is warranted. We make this case from both a *cost* and *capability* perspective.

Approved for public release; distribution is unlimited.

Capability: PHIP sensor spectral responsivity is narrow-band and can be seamlessly tuned across the mid-wave infrared (MWIR), enabling multicolor arrays that will enhance detectivity of IRST systems. For example, some state-of-the-art seeker systems rely on two InSb focal plane arrays (FPAs), each observing the scene through a narrow-band filter. One band is centered on the target emission, while the other subtracts a background signal to reduce noise and false alarm rate. A complex solution (two FPAs and cold filters) can potentially be replaced by a *single PHIP array* with no additional filtration where some pixels are tuned to the peak target emission and some adjacent ones are allotted to a background band.

Cost: PHIP technology is designed to be seamlessly integrated with standard silicon processing flows. Our team has kept CMOS thermal budgets and processes foremost in mind when designing the PHIP. The active layers are deposited using a proprietary high-power impulse magnetron PVD process which has both high throughput and low substrate temperature requirements. The ability to directly deposit the active layer on silicon removes a significant barrier to direct integration with a CMOS ROIC wafer. In the future, PHIP arrays can be built without costly, low-yield hybridization steps, potentially reducing imager system cost by an order of magnitude and allowing proliferation of MWIR imagers at the individual warfighter level.

The successful Phase I program confirmed many of the key scientific hypotheses behind the PHIP technology and has laid the groundwork for further optimization of sensor design to meet DoD needs. Our team envisions extension of the PHIP architecture using more sophisticated light collection techniques to establish a baseline performance metric that will allow competitive benchmarking of the technology. The Phase I program began with a 25 July 2017 kick-off meeting and concluded 15 July 2018. No Phase II follow-on funding has been allocated.

Approved for public release; distribution is unlimited.

2. BACKGROUND

Using novel materials and device geometries unique to 3FM we propose a sensor technology that overcomes the grand challenge of direct ROIC integration of IR materials by exploring transduction pathways between mid-wave infrared plasmonic excitation in a IR metal and a measureable electric signal. 3FM is a spin-off from North Carolina State University's (NCSU's) Electronic Oxide research group.

The research is framed by boundary conditions of high-temperature operation (>200 K) and consistency with monolithic integration, with a device design that can sense multiple narrow-bands of IR light simultaneously. Achieving these goals will substantially impact the performance metrics of IR imaging systems, particularly when cost/performance tradeoffs are considered. While the detection possibilities explored are born of fundamental discovery science, there is a substantial preliminary data set that proves the detector concept.

The Electronics Oxide Group at NCSU, from which the founders of 3FM evolved, recently developed new formulations and methods to synthesize doped CdO in which carrier concentrations spanning low 10^{19}cm^{-3} to mid 10^{20}cm^{-3} are sustained with electron mobility values between 400 cm^2/V·s and 530 cm^2/V·s.[1] The combination of carrier concentration and mobility are unprecedented in existing materials, even exceeding what is possible in high mobility semiconductors like InAs and GaAs at comparable carrier concentration. These unique electronic properties present new opportunities for direct and low-loss coupling to MWIR radiation. Doped CdO is positioned to complement the current palette of IR materials and provide new solutions to mid-wave detection. We intend to exploit these properties and demonstrate how they can facilitate DoD-specific sensor needs.

2.1 IR Plasmonics

Plasmon polaritons in the near- and mid-IR portions of the electromagnetic spectrum present interesting opportunities for IR optoelectronic technologies based on conductive metal oxides (CMOs). A limiting factor associated with most conductive oxides, however, is low carrier mobility, especially at carrier densities above 10^{19} cm^{-3}. These mobility limits lower the quality factor of optical modes and erode the performance of potential optoelectronic devices. If, for example, the accessible mobility range was increased by one to two orders of magnitude, conductive metal oxides could impact several IR technologies.

One such IR technology of current interest and technological importance is based on the concept of hot carrier injection or IPE. Figure 1 illustrates the general process where incident IR light couples to free electrons in the grey conductor. A proportion of these electrons has sufficient energy to be injected across an interface into an adjacent material, such as a Schottky barrier formed by the absorbing conductor and a semiconductor. ***Most importantly, the regulating factors for injection is the incident photon energy and the band lineup between the two materials, as opposed to the semiconductor band gap.*** If the semiconductor band gap is greater than or on the order of 1 eV thermal excitation across the bandgap will be very low at room temperature, allowing one to detect the hot carriers with low background noise. This

Approved for public release; distribution is unlimited.

phenomenon creates an exciting opportunity for MWIR detectors by exploiting the unique light matter interactions enabled by plasmonic modes.

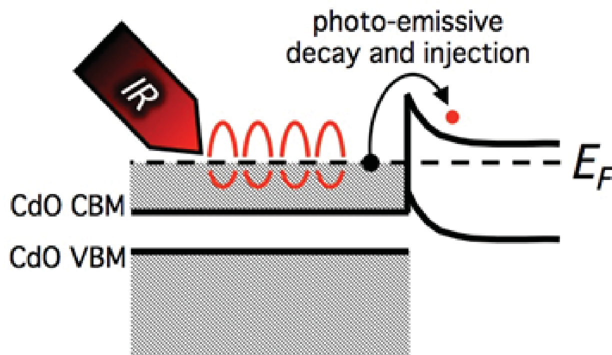

Figure 1: Schematic Illustration of Photoemission by Hot Carrier Injection from Plasmonic Decay

The concept is known to the nanophotonics community, and such devices were fabricated and first demonstrated by the Halas Group at Rice[2]. In their case near-IR light couples to a nanopatterned Au layer and excites a localized surface plasmon. During the plasmon decay process, hot electrons are injected across a Schottky barrier into the conduction band of Si where they are collected as photocurrent. While this device works, there are material property limitations that reduce the efficiency to values ~ 0.2%. These include:

1) *IR-plasmons in Au are fundamentally lossy;*
2) *Only hot electrons generated very close to the semiconductor interface can be collected;*
3) *Due to the momentum directionality of plasmon-induced hot carriers in metal nanostructures, only a fraction of hot electrons have trajectories perpendicular to the interface*[3]*;*

The most restrictive limitations above arise because electron mobility in metals is low, Au-interband transitions introduce additional loss mechanisms, and plasmonic coupling to IR wavelengths in conductors with 10^{23} cm^{-3} carriers requires complex nanostructuring (typically via e-beam lithography) and couples inefficiently to IR light (low absorbance). These limitations are openly discussed in several recent plasmonic review articles, and a consensus opinion suggests that overcoming them requires an engineered material with a combination of properties that are to varying extents mutually exclusive in most known conductors.

2.2 R:CdO – an Enabling Plasmonic Infrared Material

Recent work at NCSU (2017) produced a donor-doped R:CdO process using 3^+ cations (R = Ag, Y, In) with electrical and optical properties that are engineered for light-matter interaction in the mid-IR. Transport properties for doped CdO are summarized in Figure 2. Most importantly, electron mobility values approaching 500 $cm^2/V{\cdot}s$ are possible at carrier densities which couple to long-wave and mid-wave IR light via plasmonic or epsilon near zero (ENZ) modes. This combination is simply unprecedented in other known materials.

Approved for public release; distribution is unlimited.

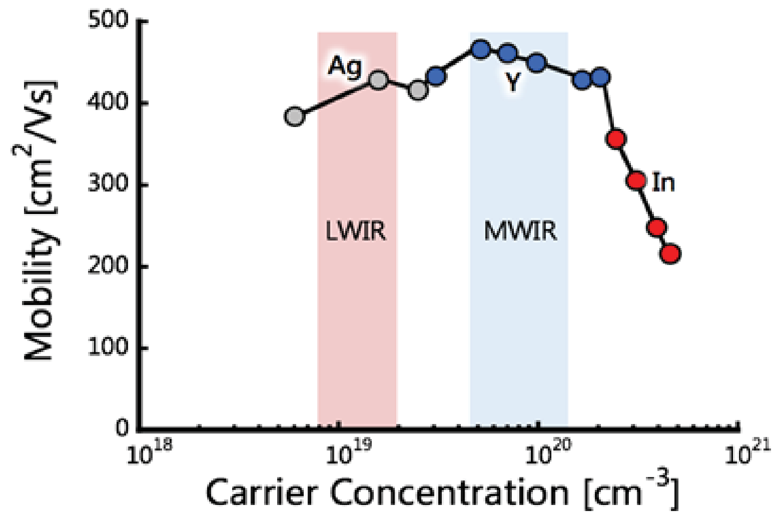

Figure 2: Carrier Density and Mobility for Sputtered CdO Thin Films Donor-doped with various Cations

Note that mobility values approach 500 $cm^2/V{\cdot}s$ carrier densities between 10^{19}/cc and 10^{20}/cc

We identify donor-doped CdO as an enabling material for mid-wave IR technologies for the following reasons:

1) *CdO behaves as an ideal Drude conductor at energies below its bandgap, thus plasmonic losses are very small owing to its high carrier mobility. The Drude behavior of R:CdO has been verified over the mid-IR energy range by infrared variable angle spectroscopic ellipsometry (IR-VASE);*
2) *The carrier mobility in CdO (in the $10^{20}cm^{-3}$ range) is 10 to 30 times higher than in other hosts (e.g., ZnO, ITO, etc.) which translates to longer-lifetime polaritons, carrier diffusion lengths and improved hot carrier generation; and*
3) *R:CdO can be grown at temperatures below 350°C on silicon substrates using PVD methods (reactive sputtering), offering direct CMOS compatibility and the scaleability inherent to mature CMOS processes.*

2.3 CdO Light Matter Interaction – ENZ Modes

Thin films made of metals, doped semiconductors, or polar materials can support plasmon- or phonon-polariton eigenmodes (i.e. intense optical absorption events). The most common mode discussed in the literature is the surface plasmon polariton (SPP). This mode has been successfully integrated into opto-electronic technologies. However, due to the carrier concentration range accessible in CMOs, access to other eigenmodes becomes practical. 3FM's technology is based on the epsilon-near-zero mode (ENZ mode), which is unique to optical systems that employ deep subwavelength structures. In the following section, we introduce the ENZ mode and in particular the characteristics that make it interesting for detector applications. The treatment below is by necessity high level, but an excellent review has been reported by Campione et al.;[4] where the dependence of ENZ modes on thickness, carrier density, and mobility are explained in detail. From the work of Campione and others we identify several key points:

Approved for public release; distribution is unlimited.

- ENZ modes occur at a resonant energy that is approximately equal to the zero point of the real part of the dielectric function, the frequency is given by:

$$\omega_p = q\sqrt{\frac{n_e}{m_e \varepsilon_0}} \quad (1)$$

$$with\ n_e = carrier\ density, m_e = effective\ mass, \varepsilon_0 = free\ space\ permittivity, and\ q = elementary\ charge$$

- In CdO we can control carrier density over 4 decades, this enables us to tune the ENZ energy (*i.e.*, ω_p) through the entire mid-wave portion of the IR spectrum.
- Models for ENZ modes, in accordance with experimental data show that perfect absorption occurs at low thickness values relative to the considered wavelength. For mid-IR energies and common transparent conducting oxides (TCOs), typical values are less than 150 nm for perfect absorption. Ultimately, light is confined into structures that are far thinner than the coupling photon wavelength. This results in very large local electric fields, and in turn, higher net excited electron energies as compared to other plasmonic modes. Figure 3 provides a cartoon illustration showing the extent of "photon compression".

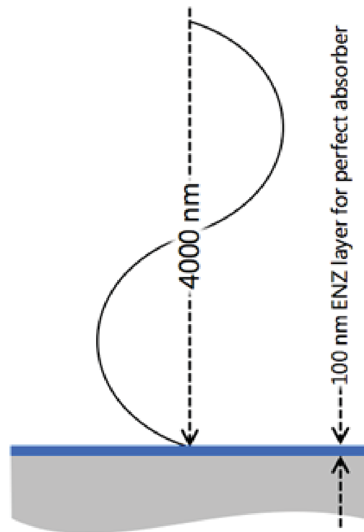

Figure 3: Illustration showing the Relationship between IR Wavelength and the Thickness of ENZ Layer in which perfect Absorption occurs

- The ENZ mode couples through collective oscillations of energetic electrons among a reservoir of electrons in the conduction band of the CdO, adding energy to the e- population above the bandgap. As such, thin films that support ENZ modes are efficient light absorbers for an electronic detection device.

Approved for public release; distribution is unlimited.

We experimentally demonstrated seamless tunability of the CdO ENZ mode over the 3-5 µm band (total range 2-9 µm). Perfect absorption can be achieved in films with thicknesses < 150nm for 5 µm wavelength, demonstrating the optically confining properties of the CdO ENZ modes.

2.4 Internal Photoemission

IPE is an important light-matter interaction where optical absorption creates free electronic carriers. IPE is elegant in its simplicity as it requires only a Schottky barrier at a metal-semiconductor interface. The standard IPE theory was described by Fowler (1931) and extended by Vickers (1971) and Archer and Cohen (1973). The process has been employed for infrared detection and imaging based on Si integrated circuits (ICs) and devices.

IPE occurs by free-carrier absorption of IR light in a metallic layer, consequent production of excited electrons, and subsequent injection of these hot electrons over the potential barrier formed at the metal-semiconductor interface. Si-based Schottky-barrier IPE focal plane arrays represent the pioneering technology for large-area, high-resolution near infrared (NIR, 1 to 3 µm), and mid infrared (MIR, 3 to 5 µm) detector applications. PtSi/Si Schottky barrier detectors (SBDs) are the most established SBD materials system for mid-wave energies. Other common material systems are Pd_2Si (NIR) and IrSi (long-wave infrared (LWIR)).

Schottky photoemission is independent of factors like semiconductor doping, minority carrier lifetime, and alloy composition. As such, *spatial uniformity* is far superior when compared to other detector technologies; being only limited by the geometric definition of the detectors. This is why silicide SBDs can be an attractive and much more reproducible alternative to HgCdTe, quantum-well infrared photodetectors (QWIPs) or Type-II strained layer super-lattice (T2SL) FPAs for infrared thermal imaging. Excellent uniformity enhances IR performance by minimizing the need to compensate pixel response using external electronics and temperature references.

However, there are obvious drawbacks to the Si based IPE technology. The effective quantum efficiency in the 3–5 µm window is very low, on the order of 1%. Detectivites of PtSi detectors are about an order of magnitude below the state of the art detectors for the MWIR band (D* typically 1E9-1E10 Jones). However, useful sensitivity is obtained by near full-frame integration in arrays. To compensate for low quantum efficiency and high dark currents, Schottky-barrier photoemissive detectors operate at cryogenic temperatures. The low quantum efficiency is due to:

- Ineffective excitation/injection of photo excited carriers into the semiconductor substrate.
- Low carrier lifetimes in the metallic layer (silicide).
- Non-tunable broadband absorption in a single material.
- Non-directional electron emission: many exited electrons accelerated away from semiconductor interface and do not contribute to a photocurrent.
- Low absorption coefficient in the silicide (high reflection losses).
- Carriers are excited at energy states indiscriminately. Many will be far below the Fermi energy, which have zero probability to overcome the Schottky barrier.

Approved for public release; distribution is unlimited.

Strategies to increase the internal quantum efficiency include thinning the PtSi film (to reflect electrons towards the interface) and introducing an optical cavity to increase absorption. A thin absorber increases the chance of successful photoemission, however this lowers overall metal absorbance and reduces the external quantum efficiency (EQE). Employing light concentration schemes like optical cavities or distributed Bragg reflectors (DBRs) will counter the reduced EQE, but add substantial complexity to the otherwise appealingly simple device structure.

Our team has replaced the silicide element in IPE detectors with a CdO ENZ absorber that overcomes or reduces these limitations. Ultimately, with CdO perfect polaritonic absorbers it is possible to retain the elegant monolithic structure and uniformity of PtSi SBDs while introducing a carrier excitation mechanism that boosts efficiency and enhances functionality.

- **Enhanced Carrier lifetime & Diffusion length:** Carrier mobility in CdO thin films is >100X higher than in metal silicides. This increases carrier lifetime and carrier diffusion lengths of the photo excited state subsequently improving the rate of excited carrier emission.
- **Directionality of electron excitation:** The ENZ mode collective electron oscillation is perpendicular to the Schottky barrier interface; creating the highest probability for emission. The high-symmetry parabolic conduction band around the CdO Γ–point imposes no limitations to the momentum distribution and directionality of the carriers in the CdO. In contrast, in SBD devices employing metallic silicides or metals, the directionality of the excited electron distribution is modified by the complex band structures in the conduction bands, further lowering the emission probability.
- **Tunable absorption:** CdO is a wide bandgap semiconductor with a phonon band around 70 meV; undoped, it is transparent to mid-wave and long-wave IR radiation. By adjusting carrier density, one can establish the plasmonic ENZ mode, and thus narrow band absorption between 2 and 6 µm. CdO offers unprecedented control over the spectral response of SBD detectors.
- **Density of states (DOS):** CdO exhibits a direct bandgap of 2.1 eV and the ENZ absorption is entirely facilitated by conduction band electrons. This limits the density of states available around the SB, and excited electrons are more likely to gain enough energy for emission. Since there is no available DOS within the bandgap, only high mobility electrons in the conduction band participate in the absorption/emission. We contrast this feature with silicide based detectors; here hot electrons far below the Schottky barrier height (SBH) can be excited with zero probability of emission. Figure 4 illustrates the band lineup between CdO and silicon, as well as the corresponding DOS. Excited e- must originate from the conduction band close to the Fermi level. This narrows the hot e- distribution towards energies sufficient for successful emission into the silicon.
- **Tailored barrier heights:** For each ENZ mode energy, the optimal Schottky barrier height can be adjusted by modifying the Si-substrate. Therefore, over the entire MWIR band, each wavelength can be extracted over an optimized barrier with maximum efficiency and minimal dark current.
- **Crosstalk:** The deep sub wavelength structure of the ENZ emitter limits optical crosstalk. In contrast with other MWIR technologies (mercury cadmium telluride (MCT), QWIP, and T2SL), where absorber regions exceed 1 µm thickness, active regions in ENZ based structures are below 200nm. Because the optical cross-section is relatively small, it is less

Approved for public release; distribution is unlimited.

likely that photons incident on a particular pixel will be transmitted and interact with adjacent elements.

- **Process compatibility:** CdO deposition techniques, unique to 3FM, are compatible with standard silicon processing workflows. Direct integration with Si-ROICs as well as hybridization of a ROIC and silicon-based detector are feasible.

Approved for public release; distribution is unlimited.

3. PHASE I TECHNICAL OBJECTIVES

The Phase I goal is to develop a mechanistic understanding of epsilon-near-zero (ENZ) mode polariton-driven photoemission in CdO|silicon heterostructures, including a material and interface model that relates photocurrent to CdO polaritons, to dielectric conduction paths, and to band offsets. Extensive material growth and characterization has been carried out during Phase I. A modest modification of the original program of work was presented in the kick-off meeting to more closely align the project with DARPA and WIRED program goals. The Phase I effort sought a better understanding of the properties of the CdO|Si Schottky barrier and the performance of a prototype IPE detector. We believe the Phase I effort resulted in a successful technology demonstrator. Phase II follow on funding was originally allocated to test the performance envelope of the device after proof-of-concept. A summary of the technical goals is presented:

- *Measure the Schottky barrier height of the CdO|Si diode. SBH establishes long-wave cutoff in these devices and is one of the most important performance parameters.*
- *Understand and quantify the dark-current in CdO|Si heterostructures - how do deposition and processing parameters affect the observed dark-current.*
- *Demonstrate the ability to tune the resonance and absorption over the entire MWIR band in non-epi CdO films by varying the doping concentration.*
- *Improve the device performance by addressing diode electrical characteristics and light coupling to the active layer.*
- *Design readout circuitry compatible with PHIP detector capacitance and junction resistance to amplify the photosignal and allow for biased measurements.*
- *Measure spectral response of PHIP detectors and confirm that absorption is correlated with response profile.*

Approved for public release; distribution is unlimited.

4. PHASE I PROGRAM RESULTS

The Phase I program resulted in a number of improvements to the PHIP design and a significantly better understanding of the nature of the SBD formed at the junction of CdO and silicon. The following section reports the significant findings of the effort organized around the 6 overarching technical objectives assigned in the previous section.

4.1 Analysis of SBH, Long-Wave Cutoff, and Diode Performance

The Schottky barrier height of CdO|Si diodes was measured using several methods for completeness and validation. Initially, the band line-up of CdO and silicon was measured using XPS. Although this result will provide an estimate of the barrier height in the Schottky limit (where the difference in affinity defines the barrier), it likely over-predicts the true barrier height between these materials. CdO is a degenerate n-type semiconductor with an indirect gap of approximately 1.2 eV. We anticipate a Type-II staggered band alignment for the CdO|Si heterojunction. We use this data in conjunction with the XPS determined valence-band offset to sketch the band line-up for CdO films on silicon in Figure 5. The measured 0.47 eV conduction-band offset implies a large Schottky barrier height although in principle this value will be reduced due to interfacial defects and other non-idealities. SBHs of greater than 0.45 eV as estimated using XPS push the longwave cutoff into the near-IR (~2.7 µm).

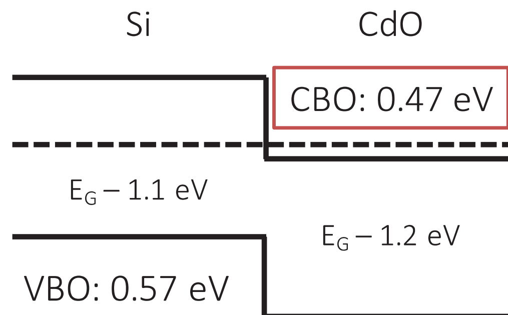

Figure 5: Schematic of the Band Lineup Measured by XPS for a CdO Film on Silicon
A measured valence-band offset of 0.57 eV produces a conduction-band offset of 0.47 eV in the Schottky limit.

An early program effort to understand the effects of silicon surface modification showed significant changes in rectifying behavior of CdO|Si diodes. Measurement of true SBH was frustrated by parasitic effects but future studies will examine the effects of Si surface treatment on the spectral response and cutoff wavelength. Figure 6 illustrates the effect of silicon modification by chemical stripping and Ar^+ ion-beam bombardment on SBD I-V performance.

Samples receiving no treatment were the most rectifying while the I-V characteristic became significantly more symmetric for samples that were ion-bombarded prior to CdO deposition. The range of I-V responses in Figure 6 suggests that modification of the SBH is possible using surface treatments. Recording I-V response from room-temperature to ~100°C allowed for extraction of some diode characteristics. A linear fit of the current response at low forward biases can produce estimates of SBH as well as any non-idealities like series and shunt resistance.

Approved for public release; distribution is unlimited.

These analyses suggest that the above devices have large series resistances on the order of 1-100 kΩ. Coupled with high ideality factors, parasitic resistance obfuscates true SBH and makes estimation of cutoff-wavelength, and even simple diode characteristics like dark current, more difficult.

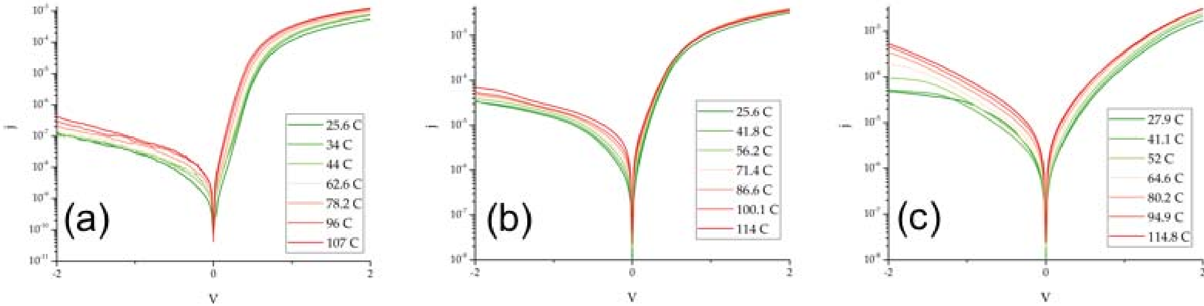

Figure 6: Temperature Dependent I-V Properties of CdO-Si Heterojunctions for (a) As-received Silicon; (b) Oxide Strip and Clean; and (c) Ion-beam Modified

To better estimate the barrier height in actual PHIP devices, the team also used forward and reverse biased temperature dependent I-V data. Temperature dependent I-V data was gathered at the Mid Infrared Characterization and Application (MICA) lab at Ohio State University from room to cryogenic temperatures. Figure 7 displays Richardson plot for both the forward and reverse bias condition. A linear fit of the log(JT^{-2}) versus inverse temperature gives the SBH from the well-known relation for thermionic emission:

$$J_{TE} = A^{*}T^{2}\exp\left(-\frac{q\phi_B}{kT}\right) \quad (2)$$

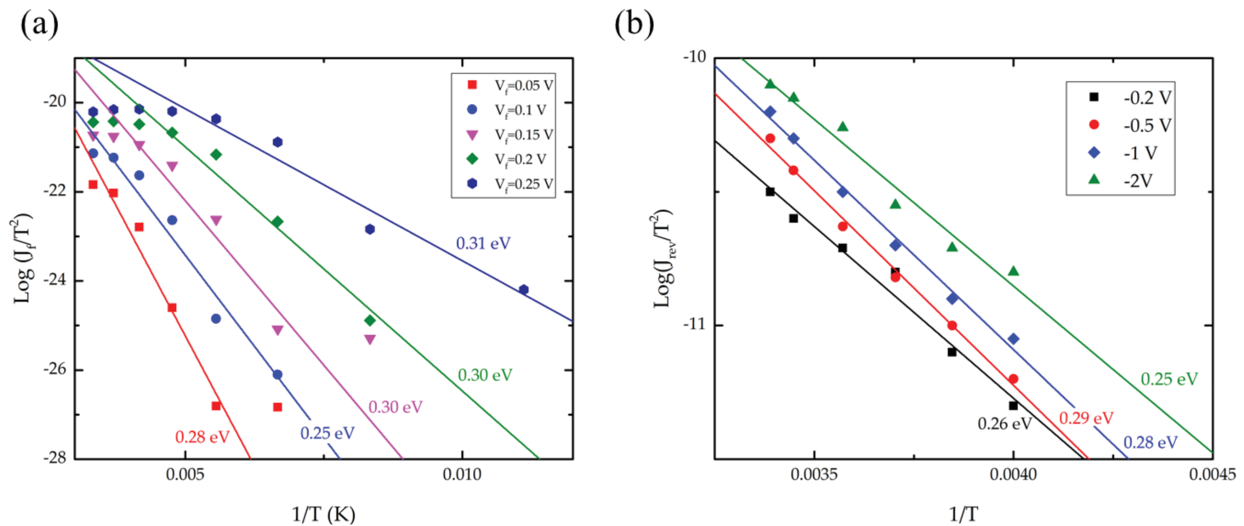

Figure 7: Richardson Plots for a representative CdO|Si SBD in Forward (a) and Reverse (b) Bias

The average SBH is relatively consistent irrespective of bias direction and we estimate the height as ~0.28 eV

Approved for public release; distribution is unlimited.

Under forward and reverse bias, we measure an average Schottky barrier height of 0.29 and 0.27 eV respectively. Several different devices converge on these average values so we estimate the barrier to be approximately 0.28 eV, pushing the long-wave cutoff to 4.4 µm. This value allows access to most of the 3-5 µm MWIR atmospheric transmission window. We note that techniques to lower Schottky barrier height in silicon diode are possible, including silicon surface treatments and delta-doped layers near the barrier. Most interestingly, the narrow-band spectral response of PHIP devices can potentially allow for optimal extraction over a designed barrier height - a possibility which will increase SNR for an optimized sensor. For example, should the imaging system need to work at 5 µm, the surface of the silicon substrate could be highly-doped which effectively reduces the barrier height. Alternatively, SiGe epitaxial layers could allow a potentially tunable Schottky barrier height within the MWIR energy range.

4.2 Understanding Dark Current in PHIP Devices

The effective signal-to-noise ratio of an IR detector is fundamentally a question of the dark-current allowed by the device. PHIP based detectors typically demonstrate very low dark current densities even at room temperature. Figure 8 plots dark I-V from 60-295 K for a typical device. At room temperature and at a moderate operational bias of -1V, dark current does not exceed 5E-5 A cm^{-2}. Compared with state-of-the-art high operating temperature (HOT) MCT diodes, which often have room temperature dark currents in excess of 10^{-2} A cm^{-2}, this result is still exceptional. Low dark current levels in PHIP detectors are promising for low noise operation and potentially for HOT detectors. All of the constituent materials in the device have bandgaps in excess of 1 eV and no carriers should result from super bandgap thermal excitation. We note that the performance results in Figure 8 in no way represent the ultimate capability of the PHIP architecture. While significant progress has been made during the 1 year program, surface passivation and other common techniques to reduce leakage currents have not yet been explored. For application where cooling requirements are constrained, the PHIP may represent an enabling technology.

Approved for public release; distribution is unlimited.

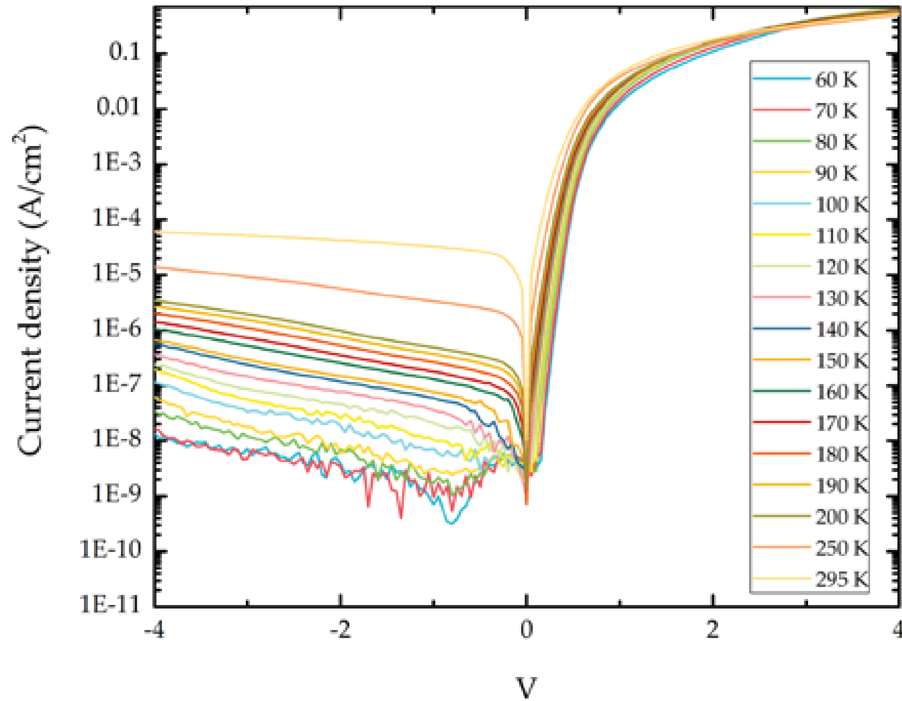

Figure 8: Temperature Dependent Current Density vs. Voltage for a Representative CdO|Si Heterojunction

4.3 Tuning of Optical Resonance across the MWIR

Prior to the start of the DARPA/AFRL program, CdO deposition was performed in ultra-high vacuum (UHV) conditions within a modified oxide molecular beam epitaxy (MBE) system. A key finding of the research group at NCSU/3FM was that deposition could be performed in a reactive sputtering environment which improved throughput but also allowed for *high quality, non-epitaxial layers*. Optical electrical properties had previously been measured only on epitaxial layers grown on sapphire and MgO substrates. Our team observed that similar material quality, assessed by the doping control and electron mobility along with sharpness of the ENZ absorption, can be achieved when fiber textured CdO was deposited on a SiO_2 or Si substrate. The deposition is accomplished in the custom-built multi-magnetron reactive sputtering system illustrated in Figure 9(a). A relatively new pulsed-direct current (DC) sputtering configuration was used to increase the self-ionization fraction and increase rate while maintaining oxygen content in the sputtered film. Doping is controlled separate from the Cd flux by adjusting radio frequency (RF) power to the dopant gun. Films deposited in this fashion on silicon had excellent electrical properties that allow for high-q ENZ resonances across the MWIR. Carrier concentration and electron mobility are plotted versus film thickness for lightly-doped In:CdO films on silicon in Figure 9(b). For relevant PHIP device thicknesses (> 50 nm) the mobility exceeds 250 $cm^2V^{-1}S^{-1}$ which is more than sufficient for a high quality ENZ absorption.

A series of films were prepared to demonstrate the ability to tune the ENZ resonance in non-epitaxial layers on silicon. Films were prepared in the reactive pulsed-DC sputtering configuration illustrated in Figure 9(a) and free carrier concentration was modified by adjusting the Influx provided by the dopant gun. ENZ absorption was characterized using IR spectroscopic

Approved for public release; distribution is unlimited.

ellipsometry on as-deposited layers – while annealing sharpens the ENZ resonance, it also can result in the formation of an insulating oxide layer at the interface. Spectroscopic data depicting the measured ENZ absorption is summarized in Figure 10. Care was taken to ensure that the films in this study were prepared in the same fashion that CdO layers would be deposited for actual PHIP device fabrication. The results indicate that ENZ absorptions of similar quality factor are attainable on silicon substrates and that perfect IR light absorption is possible in non-epi layers. We consider this demonstration integral to the PHIP device concept, where a designed absorption signature can be fabricated by varying the free carrier concentration in the CdO layer.

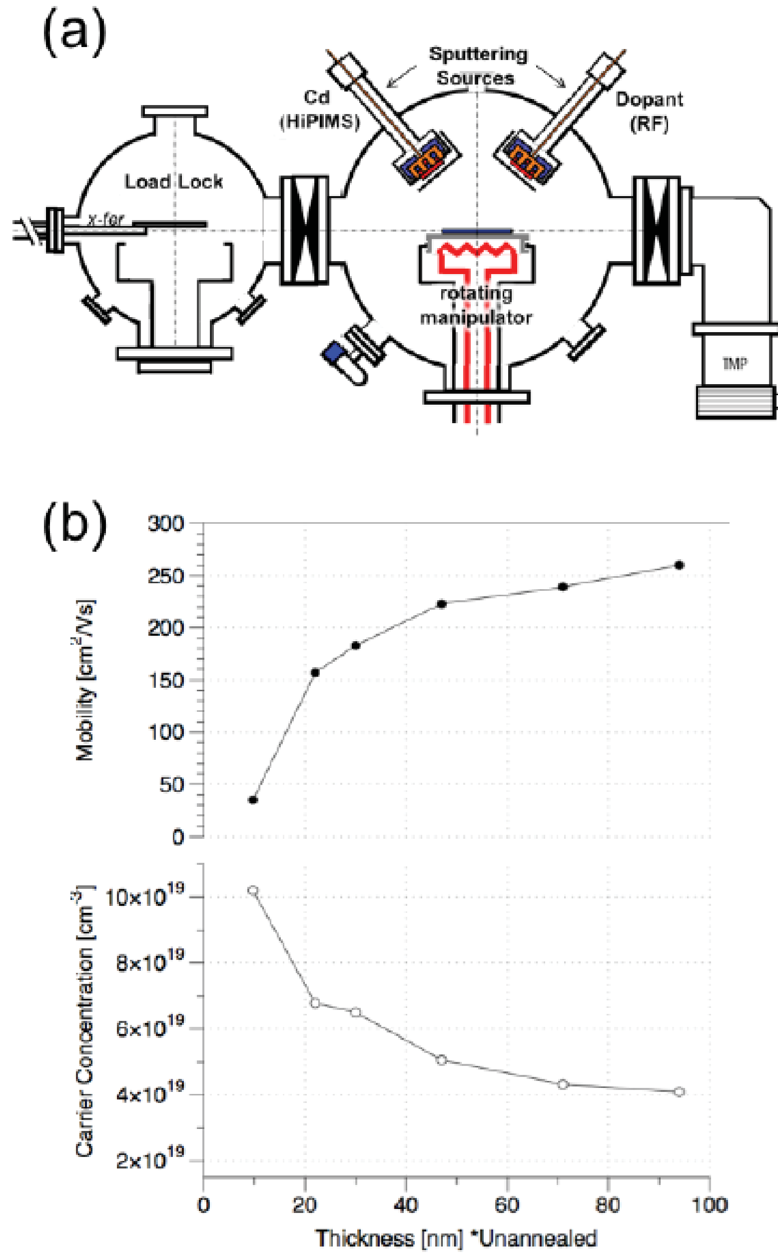

Figure 9: (a) Dual Magnetron Reactive Sputtering System for CdO Deposition and (b) Carrier Concentration and Mobility for Sputtered Films on Silicon

Approved for public release; distribution is unlimited.

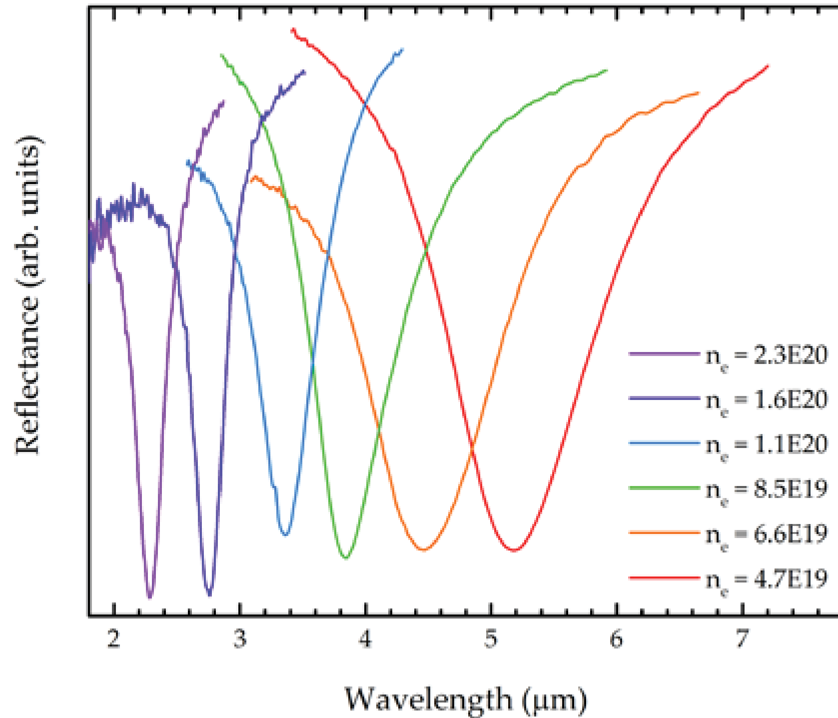

Figure 10: Reflectance measured by IR Ellipsometry for a Series of Films will varying Carrier Concentration on Silicon

Tuning of resonance possible from 2-6 µm

4.4 Improving Device Performance

During the course of the 1-year program, efforts to increase device performance centered on reduction of diode parasitics and enhancing light coupling efficiency. Locked-in photocurrent in photovoltaic mode (0 V bias) was used as an evaluation metric for device performance across several designs. The measurement setup is illustrated in Figure 11. PHIP devices with polished backsides were contacted in a two-terminal configuration and the output was detected using a SRS810 lock-in amplifier or I-V was simply read using a Keithley 4200 semiconductor analyzer. The device was illuminated with a halogen broad-band IR lightsource which was filtered with a Ge long-pass window to exclude radiation below 2 µm. The light was optically chopped at frequencies ranging from 100-600 Hz. Although this setup lacks the ability to characterize the true spectral response of the sample, it serves as a useful first check of relative performance from device to device. Significant effort was made to reduce system electrical noise due to cabling and vibration and ensure that observed signal-to-noise ratio (SNR) was not instrument limited. Using the above described measurement as metric, device performance improved 50x from our teams first evaluation at OSU's MICA lab in December 2017 to program end in July 2018. A summary of the most important improvements is chronologically presented in Figure 12.

Approved for public release; distribution is unlimited.

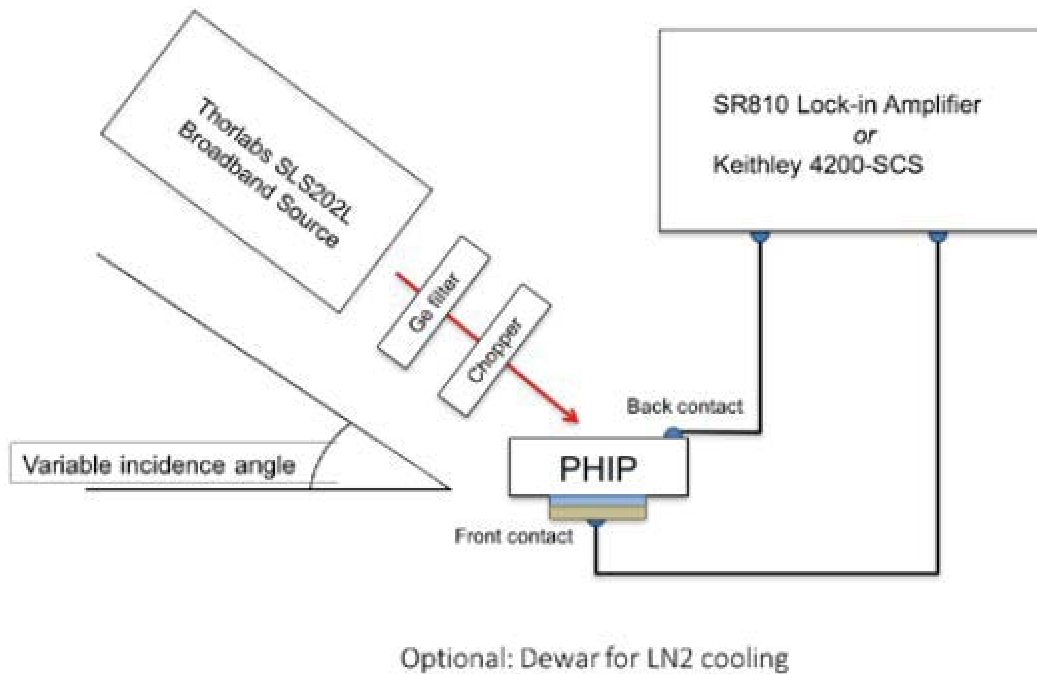

Figure 11: Typical 3FM Measurement Setup for PHIP Tests
Locked-in photocurrent is measured using a device illuminated by chopped and filtered broad-band IR light.

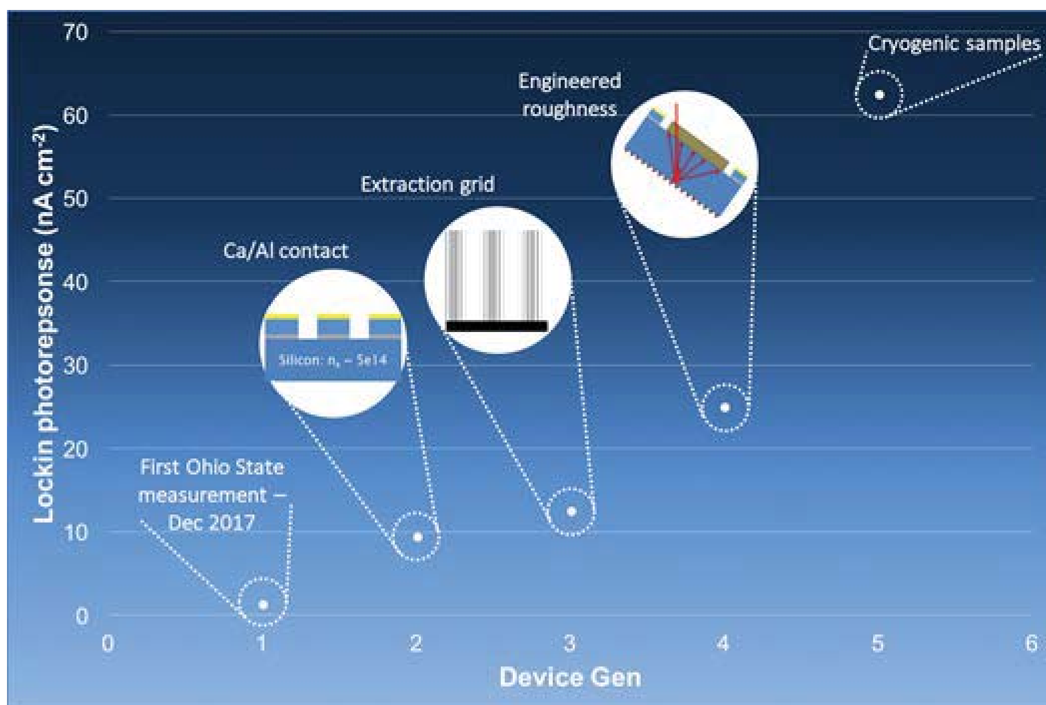

Figure 12: PHIP Device Photoresponse Improvement over Program Period-of-Performance
Early devices produced photocurrents of ~ 1 nA/cm² while optimized PHIP detectors exhibited current approaching 70 nA/cm².

Approved for public release; distribution is unlimited.

Overall performance was impacted by considering processing steps which affected both the diode non-idealities and the light collection efficiency. As referenced in Figure 12, this includes:

1. *Ohmic silicon contacts:* Parasitic series resistance in some early PHIP devices was a significant problem. Series resistances in excess of 100 kΩ were sometimes observed. To combat parasitic series resistance the silicon back contact was studied. A small series resistance in a Schottky diode is not a problem – but a large series resistance as indicated in our devices significantly suppress forward current as shown in Figure 13. Figure 13(a) is a technology computer-aided design (TCAD) simulation of a CdO-Si diode with SPICE parameters enabled to include series and shunt resistances. The addition of a 1.2 kΩ resistor has a noticeable effect on the observed forward current and 10 kΩ reduces current by a factor of 6.

   The most common origin of the series resistance is a poor ohmic back contact. Previous devices used In/Al contact stacks that were typically ohmic but this material no longer produces a low resistance contact with lightly doped n-type silicon. A proprietary Ca/Al stack (illustrated in Figure 13(b)), however, shows promise in reducing the contact resistivity of the back electrode and is ohmic over the entire measurement range. These contacts are prepared on BOE stripped silicon by thermal evaporation and sputtering. First, a thin 30-50 nm layer of pure Ca metal is evaporated at high vacuum (<1e-6 Torr) to ensure no oxide is formed. The Ca layer is capped in-situ with a thick (150-500 nm) thermally evaporated Al layer. Finally, Au or another noble metal is sputter deposited to seal the stack and provide a chemically resistant surface for further patterning steps. These back contacts constitute a significant improvement over previous designs and, most importantly, *are prepared at room-temperature* which protects the underlying device. Figure 13(c) illustrates the ohmic behavior of the new contact and the significantly reduced resistivity.

   Devices prepared with these new ohmic contacts displayed significantly improved performance as illustrated by the Gen 2 bullet in Figure 12. A 5x boost in lock-in photocurrent was typically observed and the best devices had photovoltaic mode signal in excess of 8 nA cm^{-2}.

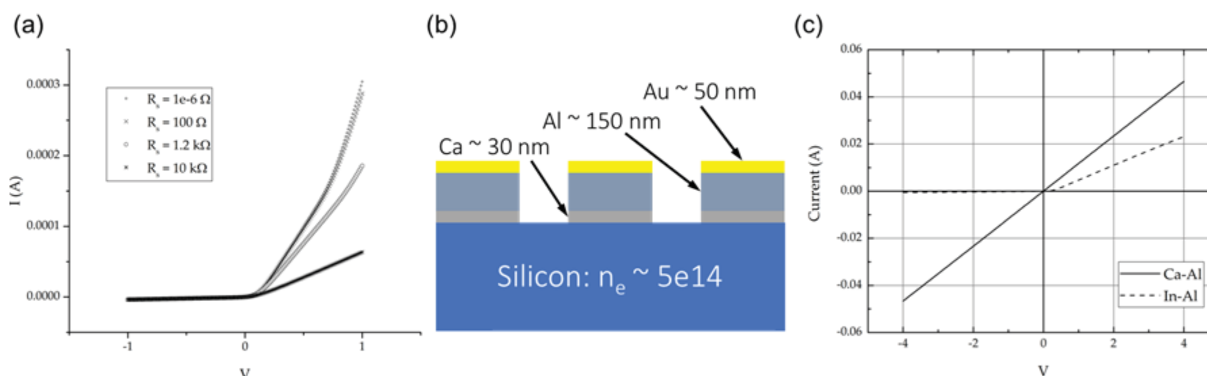

Figure 13: (a) TCAD I-V Response for CdO//Si SBD with Series Resistances of 1μΩ, 100 Ω, 1.2 kΩ, and 10 kΩ; (b) Schematic of Improved, Room-temperature Ca-Al-Au Metal Stack for Ohmic Silicon Contact; and (c) Measured I-V Characteristics for In-Al and Ca-Al back Contacts

Approved for public release; distribution is unlimited.

2. *Extraction grid development:* Ohmic Ca/Al contact metallization was integrated into an extraction grid process to increase device efficiency. The extraction grid reduced the amount of shading loss, similar to a solar cell but also decreased the hot-carrier migration length for large sized diodes. Hot carriers generated at the device edge no longer have to traverse macroscopic lateral distances, which reduces the possibility of recombination and scattering. The largest distance in this design is merely the wafer thickness (325 µm) which may of course be chemical mechanical polished to much lower thicknesses with further process development. A schematic of the extraction grid device is presented in Figure 14(a) along with a checkplot (Figure 14(b)) of the different grid geometries investigated. Each of the designs keeps the overall amount of metal the same but varies the finger spacing and finger width to optimize the process. The inclusion of an extraction grid further enhanced the observed photo current as indicated by the bullet for Gen 3 in Figure 12. Device with this configuration routinely produced lock-in photocurrent in excess of 12 nA cm^{-2}.

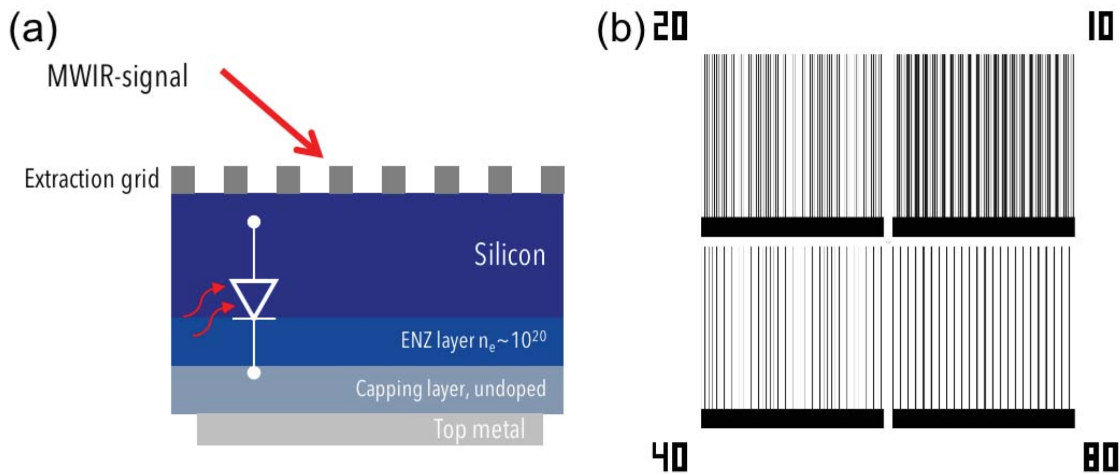

Figure 14: (a) Schematic of PHIP Single-Element Detector with Extraction Grid on Wafer Backside and (b) Checkplot of various Grid Geometries explored for Extraction Grid Optimization

3. *Enhanced light extraction through engineered roughness:* Experimentally, it is observed that only a tiny fraction of the available IR light interacts with the ENZ layer and contributes to hot-carrier injection. Most of the light simply passes through the sample or is scattered away from angles that allow a plasmonic excitation. To better understand the way in which light interacts with our sample geometry, the team experimented with a range of silicon backside polishes. Samples with highly reflective mirror finishes produced much lower photoresponse compared to those in which some hierarchical roughness remained. It was crudely determined that a uniform sanding of the backside with a particular grade of polishing media resulted in the largest observed photosignals. The hypothesized reason for the observation is twofold: 1) When light is incident on the frontside of the sample as illustrated in Figure 15, the CdO capping layer acts as an antireflective coating (CdO cap index ~ 2, Si index ~ 3 between 3-5 µm), allowing more light into the junction and 2) the backside roughness acts as an additional scattering side reflecting some light back towards the junction at angles preferential for plasmonic absorption. The inclusion of the proper amount of backside roughness in Gen 4 PHIP prototype detectors resulted in a doubling of the photocurrent, as seen in Figure 12. A 25 nA cm^{-2} signal is achievable in this architecture. Most importantly

Approved for public release; distribution is unlimited.

from a future architecture perspective, this finding confirms our suspicion that light interaction with the sample volume is likely minimal in its present form. Backside roughness is an inartful coupling geometry for plasmonic excitation and future device designs will incorporate linear and 2D gratings deposited on top of the active layers to greatly enhance light interaction with the ENZ layer.

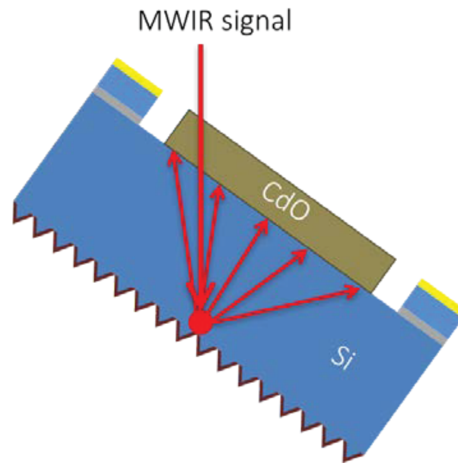

Figure 15: Schematic Illustration of the effect of Backside Roughness in Scattering Light Back towards the Interface

Proper roughness enhances the observed photocurrent.

4. *Cryogenic device designs:* Wedge mounting a PHIP sample at an optimal angle for plasmonic coupling and bonding out electrical leads to leadless chip carriers (LCCs) that can withstand multiple cryogenic cycles is non-trivial. Mechanical bonds securing the device as well as electrical wire bonds all failed when cooled to cryogenic temperatures in early prototypes. To combat this problem, the 3FM team designed a mounting process for PHIPs that was mechanically and electrically robust at every level and would allow for multiple cooling and warming test cycles in the OSU cryostat. Some of the key improvements are listed below:

    a. *Indium solder connection of precision angle ground post to LCC*
    b. *Cryogenic polyimide attachment of PHIP chip to angle post*
    c. *PVD indium deposition on CdO to enhance solderability of cathode wire contact*
    d. *Mechanical indium press contact for backside illuminated samples*

These improvements allowed the PHIP and carrier to be cooled to sub LN2 temperatures and measurements to be taken cryogenically. Samples measured at cryogenic temperatures show the highest photocurrents to-date (65 nA cm^{-2}) in our lock-in experiments. It is likely that the increase in signal is due to a reduction in the overall noise current of the device at cryogenic temperatures and not an increase in actual signal level. Regardless, the preceding PHIP innovations, financed by the DARPA/AFRL program, have greatly enhanced the signal-to-noise ratio of our devices and allowed for the first spectral responsivity characterizations of ENZ related photoemission.

Approved for public release; distribution is unlimited.

4.5 Development of a Custom ROIC

Motivation: The PHIP device represents a new detector topology with yet to be finalized electronic characteristics. It can be treated as a photoconductor, with optimum performance at moderate bias levels (<5V). For laboratory level tests, a suitable ROIC design thus will differ from standard characterization equipment typically used for photovoltaic (PV) detection devices. For a typical PV device, the generated photocurrent is amplified by a high gain trans-impedance amplifier (TIA). The TIA converts the photosignal into a voltage suitable for signal processing. This approach is not ideal for the PHIP device. Preliminary testing resulted in unstable amplification using the TIA resulting in excess noise, unsuitable for any further signal processing. This behavior was most likely caused by the large junction capacitance of the PHIP device. Higher-gain TIAs are unstable when interfaced with large capacitance sources.

This implied that the design of a custom read out circuit was needed to interface with standard equipment used for the characterization of IR detectors, such as Fourier transform infrared (FT-IR) spectral responsivity measurements.

The equivalent circuit for a generic photoconductor is depicted in Figure 16. For a PHIP device, typical values for the junction resistance **R** vary from 30kΩ (300K) to 5MΩ (77K), depending on the temperature. Figure 16 (reference I-V data), illustrates this temperature dependent change using experimental I-V data. R_L indicates the load resistance necessary to complete a circuit, which ideally is matched to the junction resistance for maximum performance.

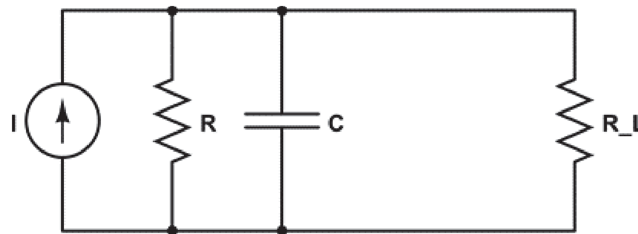

Figure 16: Equivalent Circuit for a Generic Photoconductor

The junction capacitance (C) for PHIP devices is proportional to the detector area, and can be considered high when compared to other photodetectors. The prototype PHIP devices used throughout this program exhibit junction capacitances in the 100s of nF. It is important to note that this is by no means the ultimately achievable capacitance, and the large value is mostly due to the practical, large test devices used. Scaling the PHIP to pixel dimensions below 100 µm will reduce the capacitance substantially.

In real devices, and as evident from the I-V data presented throughput the report, the I-V characteristics of the PHIP are of a Schottky-type. Thus, the diode like behavior of the device needs to be considered in the readout scheme.

The PHIP device has an unusual combination of properties for an IR-sensor. It exhibits diode-like rectification behavior, however for best performance it is interfaced to as a photoconductor. Optimal hot-carrier extraction requires biasing the structure.

Approved for public release; distribution is unlimited.

Figure 17 depicts a simple circuit to interface to PHIP photoconductors. The bias stage (detector side) allows for a controllable bias across the detector. As indicated in the schematic, an optical chopper typically modulates the light source. Upon illumination, a photosignal is created as a voltage drop across the (ideally matched) load resistor (R_L). The resulting modulated voltage is then coupled via the input stage, a 1st order filter effectively removing the DC signal offset due to the applied bias. The signal is then passed to an op-amp, to add the gain required to the signal for further processing.

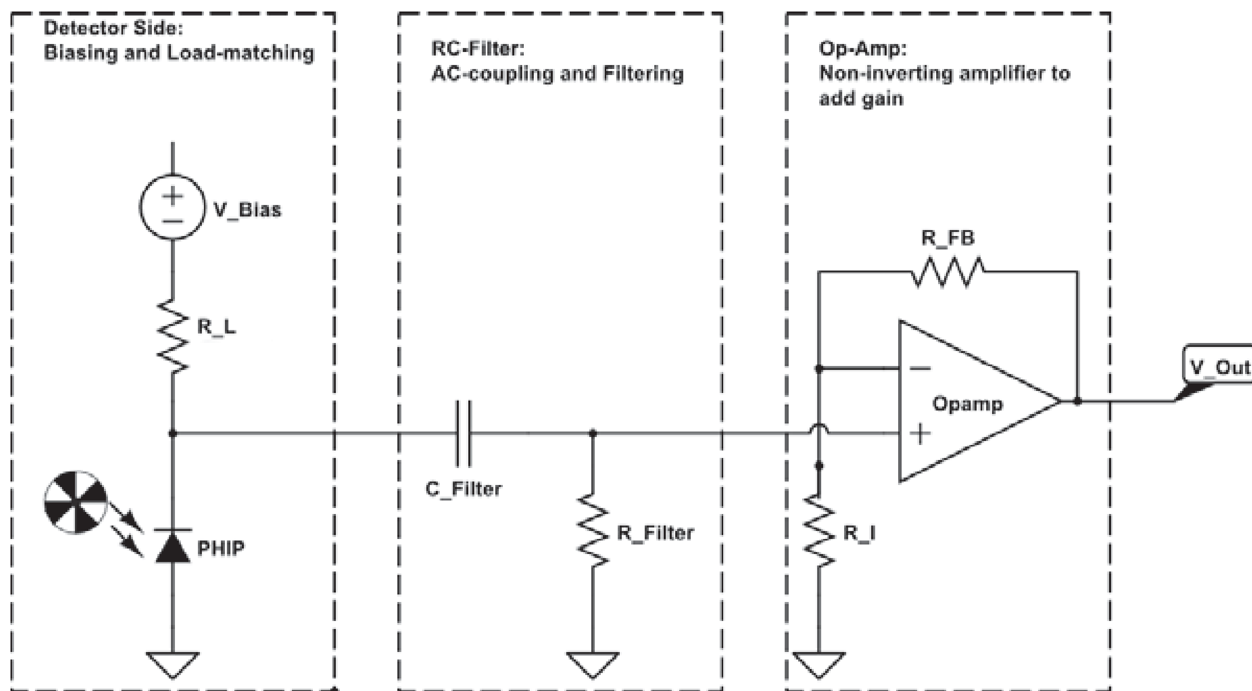

Figure 17: Simple Test Circuit for PHIP Devices

It can be divided into three functional sections (left to right): 1) The bias stage, creating the modulated photosignal. 2) The input stage, coupling to the alternating current (AC) component of the signal. This is effectively removes the DC offset applied by the bias. In combination with a resistance (R_Filter) to ground this also acts as a 1st order filter. 3) The amplifier, using a non-inverting Op-amp to provide gain to the signal. The gain is set by the feedback resistor R_FB.

This basic circuit was adapted and optimized throughout the program. Figure 18 depicts the latest iteration of the amplifier that was fabricated to aide in the PHIP characterization. This ROIC successfully interfaces with the PHIP device and provides the necessary signal levels for processing (>10mV). This two-stage amplifier allows adding sufficient gain (200dB) while maintaining stability over the frequency band necessary for spectral characterization. It further allows control over the detector bias, which can be supplied by an external voltage source or source measure unit (SMU). Figure 19 depicts the frequency behavior of the amplifier derived from the transfer function.

Approved for public release; distribution is unlimited.

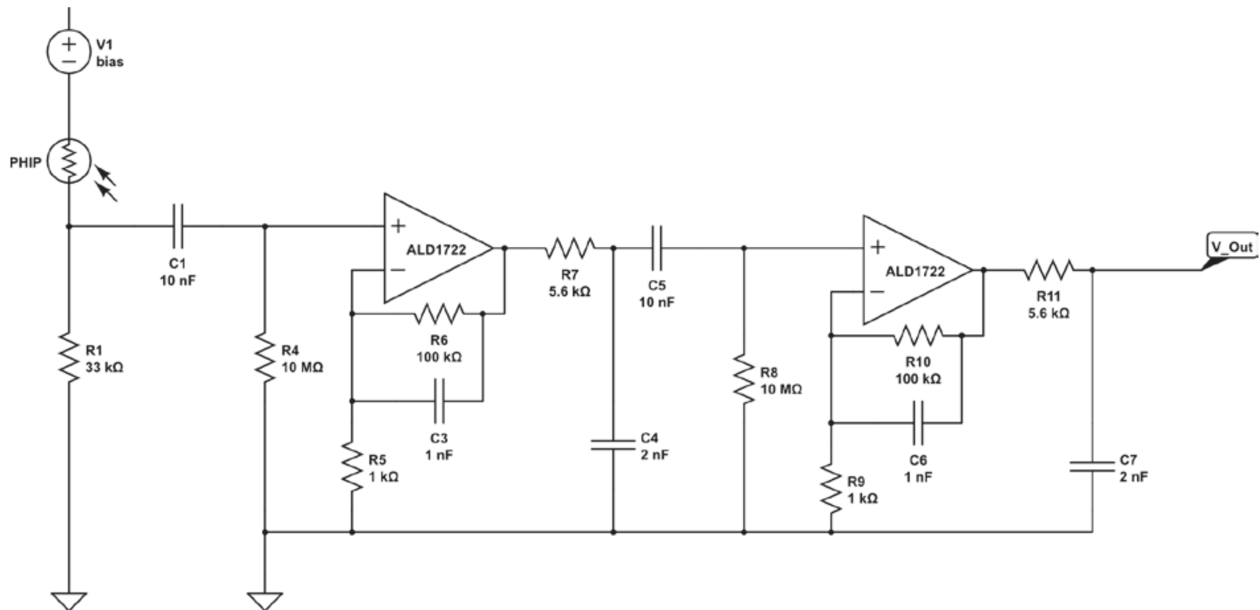

Figure 18: Schematic of the Amplifier fabricated for PHIP Measurements under Bias

R1 (input side, 33kΩ) can be exchanged with a 2MΩ resistor to match the PHIPs internal resistance at cryogenic temperatures.

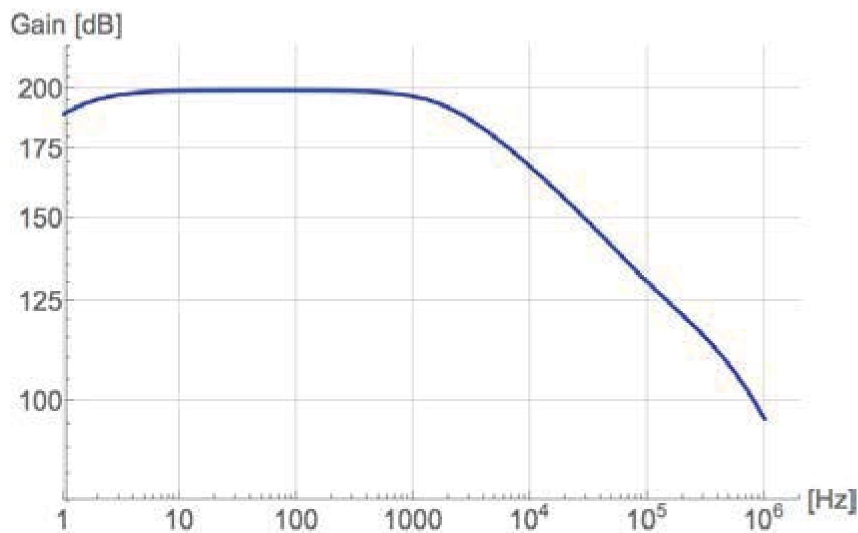

Figure 19: Calculating Transfer Function of the PHIP Readout Circuit depicted in Figure 18

The provided gain and bandwidth is compatible with the input requirements for typical FT-IR based spectral responsivity measurement setups.

Over the course of the program, we developed a versatile read-out circuit to test single-element test devices and to interface to existing equipment used in the standard characterization workflow of IR detectors. Our collaborators at OSU where able to interface test devices into their spectral response measurement workflow using the above amplifier.

Approved for public release; distribution is unlimited.

Outlook: Digital imager architectures are dominated by in-pixel readout stages containing analog-integrator pre-amplification and a posterior sampler-and-hold. In the case of large IR FPAs, straightforward input topologies like source follower per detector (SFD), direct injection (DI) and gate modulation input (GMI) are still popular because of their compactness and reduced power consumption. More complex circuit techniques like buffered direct injection (BDI) and capacitive transimpedance amplifier (CTIA) offer higher performance by providing excellent bias control, high injection efficiency, linearity and lower noise figures.

Achieving satisfactory operational performance in monolithic PHIP-CMOS focal planes poses specific technological challenges on readout circuitry. Especially:

High dark-to-signal ratios. Biased PHIP detectors deliver dark-to-signal current ratios markedly higher than from established PV-type detectors (typically orders of magnitude below unity). As a result, a direct cancellation mechanism of the dark current is needed.

Large input parasitic capacitance values. The large parasitic capacitance of the PHIP junction can limit signal bandwidth. Hence, complex in-pixel CTIAs would be required in practice to exploit the full bandwidth potential of the PHIP technology.

The basic circuit developed during this program is by design still compatible with the requirements for a monolithic CMOS FPA based on PHIP-detectors and can be used as starting point for future circuit developments.

Various ROIC designs have been fabricated for commercial use with photoconductors. There is precedence within the industry for these devices to be commercially viable, despite being a fully custom IC solution. Due to the high resistance of the PHIP, ROICs designed for high-resistance detector arrays typically found in microbolometer based FPAs can offer a suitable design starting point. These architectures allow for bias levels, offset nulling to remove DC bias offsets and integration times that we project are needed to construct a PHIP based FPA.

4.6 Successful Experimental Demonstration of the PHIP Device Concept

The concept of hot carrier generation and subsequent emission across a Schottky barrier has recently emerged as a promising alternative technology for photodetectors. The phenomenon of hot carrier generation in the context of photodetection, IPE, photovoltaics, and catalysis is increasingly getting attention in the scientific community[5]. Short wave IR photodetection has been reported using nano-patterned gold structures[6], and gold nanoparticles embedded in a dielectric matrix[7]. Silicon based IPE detection has recently been demonstrated at 1550 nm at GHz speeds[8] and in fabricated Si-pyramids using Al as the plasmonic absorber[9]. Photodetection based on plasmonic interactions operating in the mid-IR has been demonstrated utilizing hot carrier injection into-, or hot carrier generation in 2D materials such as graphene[10,11].

Several theoretical works have explored the transduction pathways for the collective electron oscillation that represents the plasmon polariton, via non-radiative decay to excited (hot) electrons. The theory is however limited to metals, an important distinction to the device presented here. Nevertheless, a number of predictions can be made from this theoretical work:

Approved for public release; distribution is unlimited.

- Hot generation rate is drastically influenced by geometry. Generally speaking, absorbing geometries that enhance the electric field confinement lead to more efficient hot carrier generation rates. This is typically achieved through establishing one or multiple of the well-studied surface plasmon polariton modes in the device.
- Hot carrier lifetimes are proportional to electron mobilities and inversely proportional to effective masses in the excited state. Thus, the bandstructure at energies around the Fermi level of the material used has the most impact on lifetimes and efficiencies. For metals, these are generally high effective mass, low mobility DOS.
- The response wavelength is tunable via geometric modifications of the absorber. For example, the well-known tunability of the absorption of Au-nanoparticles via their size allows for hot carrier generation as a response to various, tunable wavelengths. The response is, however only minimally tunable by exchanging the materials. This is due to the highly negative dielectric function of all metals at visible or infrared energies.

For the PHIP device, there are several important differences, which make it unique in the context of hot carrier generation:

- The polaritonic absorption of the ENZ mode occurs for energies with vanishing dielectric function ($\varepsilon_1 \approx 0$) in the absorber material absorption can be freely tuned over a wide energy range in the IR.
- The bandstructure around the Fermi-level can be approximated as parabolic. It is significantly simpler when compared to a metal absorber.
- The ENZ mode is a fully confined mode whose dispersion lies on the right of the light line. It was shown that this mode corresponds to a long-range surface wave mode in a deep subwavelength thin-film regime. The ENZ mode is a part of a long-range surface wave mode, which is characterized by a very large and almost constant electric field in the film. This enables hot carrier generation as a volume effect, rather than a geometries surface being the most active ("hottest") part under illumination.

Together, these differences establish the ENZ mode as uniquely suited for narrow-band absorption with subsequent hot carrier generation through non-radiative decay.

The goal of this program was to demonstrate that the ENZ absorption can be harnessed for hot-carrier generation and subsequent extraction of the carriers. Thus, to demonstrate for the first time, a hot carrier based, narrowband detector, the PHIP.

PHIP spectral response measurement: Due to the unusual electrical characteristics of the PHIP, the first measurement attempts using OSU's standard spectral sensitivity were unsuccessful. A more detailed description of the necessary development to overcome these obstacles can be found in the amplifier section. Ultimately, instrument availability limitations in combination with the ongoing amp development let us to design a simpler proof of concept experiment.

Instead of using a FT-IR based measurement approach to characterize the spectral responsivity of the PHIP, a monochromator based setup was used. This allowed for the, at the time, only viable measurement of the photosignal using a standard lock in amplification technique.

Approved for public release; distribution is unlimited.

Figure 20 depicts a schematic of the measurement setup. The monochromator available was limited to a maximum wavelength of 2400nm. This limited the accessible wavelengths substantially, however a proof of concept measurement can be performed at these energies, owing to the tunability of the PHIP. Establishing the correlation between PHIP absorption and spectral response is a viable proof of concept, even though wavelengths between 2000-3000nm are not of particular interest for real world applications. ***The involved excitation mechanism and the device structure does not change when tuning the ENZ absorption towards lower energies.***

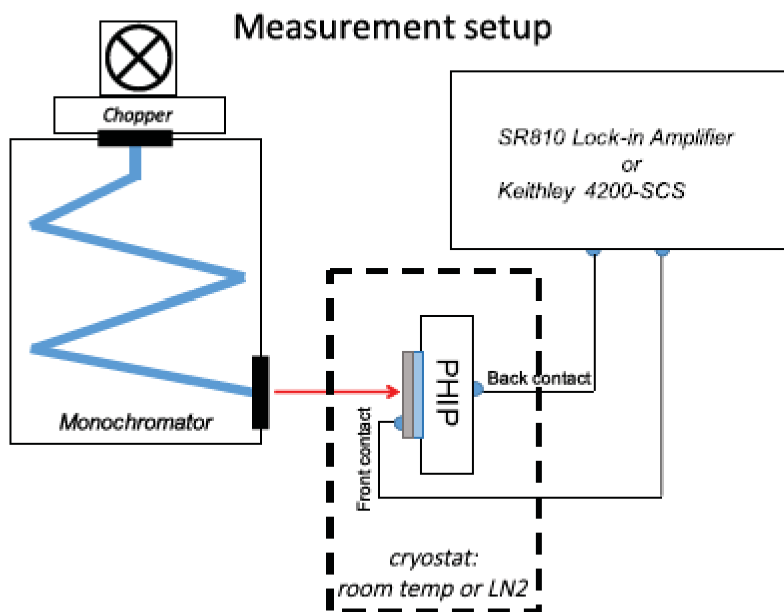

Figure 20: Schematic of the Measurement Setup used to Measure the PHIP Spectral Responsivity

To perform this measurement, a number of PHIP detectors were prepared and tuned to absorb around 2 μm. At the OSU labs, these samples were then tested for their spectral responsivity using the setup described in Figure 20. For the best data, the device was cooled using LN2. Figure 21 depicts the results plotted as spectral responsivity (top) and the devices corresponding absorbance over a comparable range of wavelengths (bottom).

Approved for public release; distribution is unlimited.

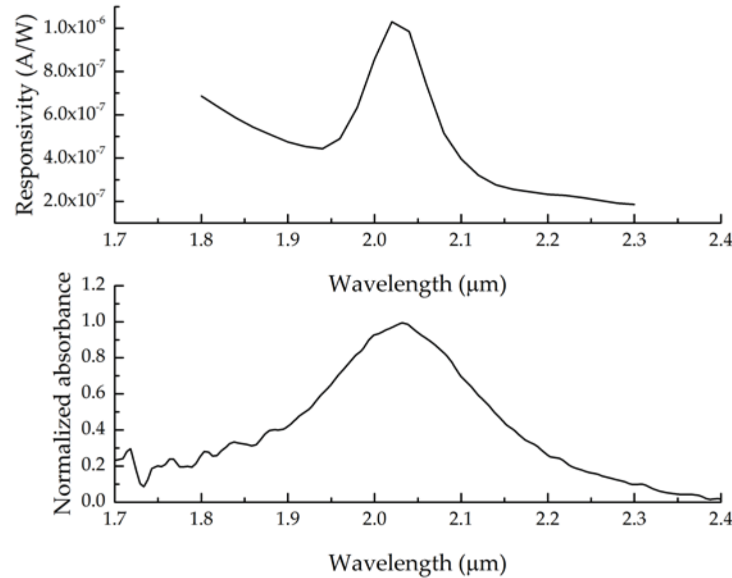

Figure 21: Measured Spectral Responsivity of a Test Device in the Infrared (top) and Measured Responsivity matches the Absorption Spectrum of the Device (bottom)
This represents the first experimental demonstration of the PHIP device and confirms its spectral response being enabled due to the ENZ mode absorption.

It can be seen, that the devices response energies match the absorption curve. This dataset represents the first experimental demonstration of an ENZ absorber based, hot-carrier infrared detector. A demonstration of the main hypothesis of this project, that the ENZ layer absorption can be used to create a tunable, narrowband response in the detector is evident from this data. The PHIP device thus allows for selecting the spectral response range of the device, by using the well-understood tuning mechanism (doping) within the ENZ layer.

The data also reveals a comparatively low absolute responsivity, of 1E-6A/W. Within the timeframe of the program, it was not possible to focus on the light gathering and field enhancement optimizations necessary to extract the maximum performance from the device. Beyond the improvements addressed within this report, there are a number of obvious design changes that can dramatically improve the absolute device performance. This program was designed to demonstrate the physics of the PHIP device and its tunability. The dataset presented here accomplished this goal.

PHIP response under bias: The instrumentation and timing constraints of the program did however not allow to perform the above measurement under bias. This was mostly due to the incompatibility of the bias stage with the setup. The last iteration of the PHIP amplifier presented in this report was tested compatible with all radiometric characterization techniques and will allow for future measurements of spectral response vs. temperature and bias of the PHIP device.

The PHIP detectors exhibit a characteristic behavior under bias, which is consistent with barrier type devices. Figure 22 demonstrates experimental data of a typical PHIP device exposed to blackbody radiation under changing bias. A turn-on voltage of >2V reverse bias is found. At

Approved for public release; distribution is unlimited.

optimal bias levels, the device response increases by two orders of magnitude. This is typical for Schottky-barrier based devices, since the applied reverse bias acts as the main driving force to extract carriers. Without a bias, such as in the spectral response dataset (see Figure 21), the only driving force to extract carriers is the built in potential difference of the Schottky junction. The measured signal levels measured for the spectral response of the device thus signify in no means the absolute performance. The data had to be recorded in a sub-optimal circuit due to the instrumentation issues detailed above.

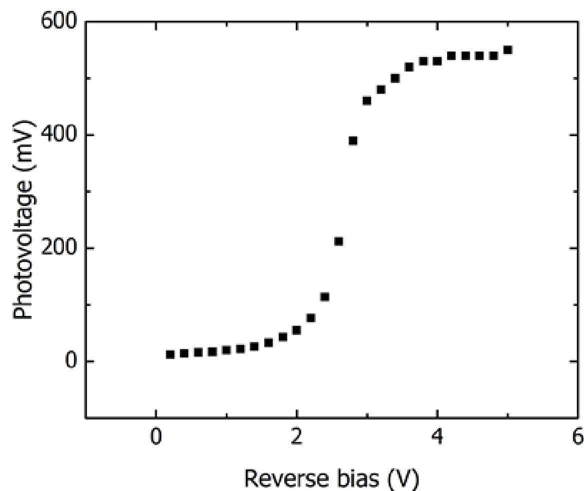

Figure 22: Bias Dependent Response of a PHIP Device

A characteristic turn-on voltage is found. The turn on corresponds to a 100x increase in the measured signal levels. This data was measured using the latest iteration of the PHIP amplifier.

In summary: the data presented in this report highlights the unique, and for the first time experimentally verified properties of the PHIP IR-detector. The unique ability of the PHIP device to harness a tunable ENZ infrared absorption for photodetection has been demonstrated. The combination of spectral response measurements and the characterized bias dependent turn-on of the device demonstrate the potential of the PHIP architecture for infrared sensing. Combined, the data suggest that the spectral response performance of the PHIP can be improved by orders of magnitude. This program thus succeeded in demonstrating the novel detector architecture of the PHIP qualitatively. The quantitative, ultimate performance limit is yet to be established.

Approved for public release; distribution is unlimited.

5. OUTLOOK FOR THE PHIP DEVICE

3FM will continue to develop the PHIP device and to incorporate all findings presented in this report. We expect to make steady progress, especially since the major hurdle of the entire DARPA/AFRL program has been solved. By developing the measurements techniques necessary to study the PHIP device, future focus will lie on optimizing the device for spectral response. We finish this report with a figure summarizing the PHIP detector technology. Figure 23 presents the advantage of the PHIP device in two panels. Panel (a) reiterates the seamless tunability of the ENZ mode absorption, which allows for a uniquely tunable, narrow band detection device. Panel (b) depicts, purposefully wavelength agnostic, how the ENZ absorption of the PHIP device corresponds to the detectors spectral response. This report includes the first experimental demonstration of this concept and lays the foundation for future development of the PHIP technology.

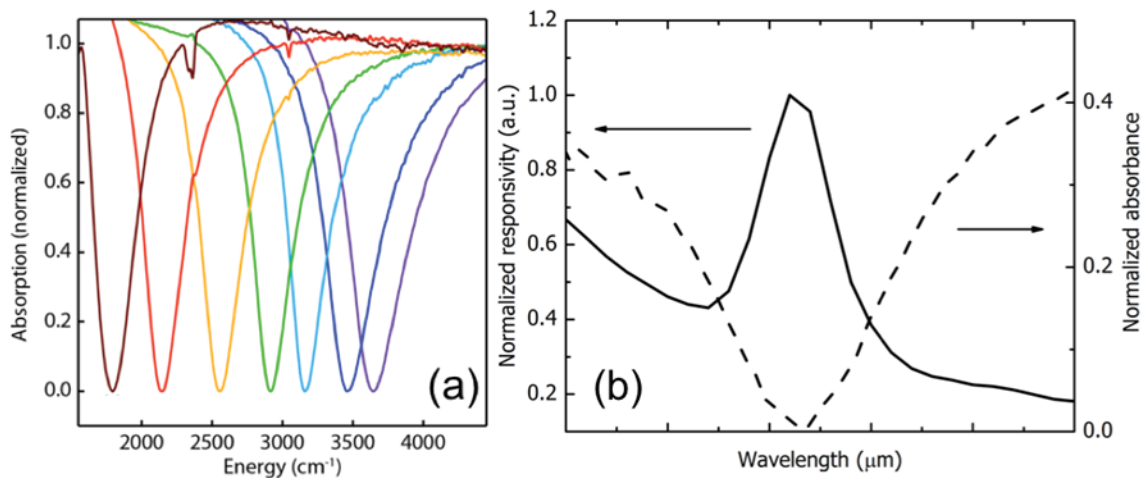

Figure 23: Advantage of the PHIP Device in two Panels

(a) Experimental narrowband ENZ absorption in multiple PHIP devices illustrating seamless tunability of the response band across the MWIR. (b) For a prototype PHIP device the absorption (dashed line) exactly corresponds with a peak in responsivity (solid). This summarized the unique ability of the PHIP device to harness a tunable ENZ infrared absorption for photodetection.

Approved for public release; distribution is unlimited.

6. REFERENCES

1. Sachet, E. *et al.* Dysprosium-doped cadmium oxide as a gateway material for mid-infrared plasmonics. *Nat. Mater.* **14,** 414–420 (2015).
2. Knight, M. W., Sobhani, H., Nordlander, P. & Halas, N. J. Photodetection with Active Optical Antennas. *Science* **332,** 702–704 (2011).
3. Knight, M. W. *et al.* Embedding Plasmonic Nanostructure Diodes Enhances Hot Electron Emission. *Nano Lett.* **13,** 1687–1692 (2013).
4. Campione, S., Brener, I. & Marquier, F. Theory of epsilon-near-zero modes in ultrathin films. *Phys. Rev. B* **91,** 121408 (2015).
5. Brongersma, M. L., Halas, N. J. & Nordlander, P. Plasmon-induced hot carrier science and technology. *Nat. Nanotechnol.* **10,** 25–34 (2015).
6. Knight, M. W., Sobhani, H., Nordlander, P. & Halas, N. J. Photodetection with Active Optical Antennas. *Science* **332,** 702–704 (2011).
7. Mubeen, S., Hernandez-Sosa, G., Moses, D., Lee, J. & Moskovits, M. Plasmonic Photosensitization of a Wide Band Gap Semiconductor: Converting Plasmons to Charge Carriers. *Nano Lett.* **11,** 5548–5552 (2011).
8. Muehlbrandt, S. *et al.* Silicon-plasmonic internal-photoemission detector for 40 Gbit/s data reception. *Optica* **3,** 741–747 (2016).
9. Grajower, M. *et al.* Optimization and Experimental Demonstration of Plasmonic Enhanced Internal Photoemission Silicon Schottky Detectors in the Mid-IR. *ACS Photonics* **4,** 1015–1020 (2017).
10. Xia, Z. *et al.* Solution-Processed Gold Nanorods Integrated with Graphene for Near-Infrared Photodetection via Hot Carrier Injection. *ACS Appl. Mater. Interfaces* **7,** 24136–24141 (2015).
11. Tielrooij, K. J. *et al.* Photoexcitation cascade and multiple hot-carrier generation in graphene. *Nat. Phys.* **9,** 248–252 (2013).

Approved for public release; distribution is unlimited.

LIST OF ABBREVIATIONS, ACRONYMS, AND SYMBOLS

ACRONYM	DESCRIPTION
3FM	Third Floor Materials, Inc.
AC	alternating current
AFRL	Air Force Research Laboratory
BDI	buffered direct injection
CdO	cadmium oxide
CMO	conductive metal oxide
CMOS	complementary metal-oxide-semiconductor
CTIA	capacitive transimpedance amplifier
DARPA	Defense Advanced Research Projects Agency
DBR	distributed Bragg reflector
DC	direct current
DI	direct injection
DoD	Department of Defense
DOS	density of states
ENZ	epsilon near zero
EQE	external quantum efficiency
FPA	focal plane array
FTIR	Fourier transform infrared
GMI	gate modulation input
HOT	high operating temperature
IC	integrated circuit
IPE	internal photoemission
IR	infrared
IRST	infrared search and track
LLC	leadless chip carrier
LWIR	long-wave infrared
MBE	molecular beam epitaxy
MCT	mercury cadmium telluride
MICA	Mid Infrared Characterization and Application
MIR	mid infrared
MWIR	mid-wave infrared
NCSU	North Carolina State University
NIR	near infrared
OSU	Ohio State University
PHIP	Photoemissive Heterostructure Infrared Photodetector
PV	photovoltaic
PVD	physical vapor deposition
QE	quantum efficiency
QWIP	quantum-well infrared photodetector
RF	radio frequency
ROIC	readout integrated circuit
SBD	Schottky barrier detector
SBH	Schottky barrier height

Approved for public release; distribution is unlimited.

ACRONYM	DESCRIPTION
SFD	source follower per detector
SMU	source measure unit
SNR	signal-to-noise ratio
SPP	surface plasmon polariton
T2SL	Type-II strained layer super-lattice
TCAD	technology computer-aided design
TCO	transparent conducting oxide
TIA	trans-impedance amplifier
UHV	ultra-high vacuum
VASE	variable angle spectroscopic ellipsometry
WIRED	Wafer Scale Infrared Detectors (DARPA program)

Approved for public release; distribution is unlimited.